



Liquid injection in a fluidised bed: Temperature uniformity

E. Milacic^{a,b}, M. Nunez Manzano^c, S. Madanikashani^{c,d}, G.J. Heynderickx^c, K.M. Van Geem^c, M.W. Baltussen^{a,b,*}, J.A.M. Kuipers^{a,b}

^a Multiphase Reactors Group, Department of Chemical Engineering and Chemistry, Eindhoven University of Technology, P.O. Box 513, 5600 MB Eindhoven, the Netherlands

^b DPI, P.O. Box 902, 5600 AX Eindhoven, the Netherlands

^c Laboratory for Chemical Technology, Department of Materials, Textiles and Chemical Engineering, Ghent University, Ghent, Belgium

^d Materials and Process Engineering (IMAP), Institute of Mechanics, Materials and Civil Engineering (iMMC), Université catholique de Louvain, Belgium

HIGHLIGHTS

- Combination of Particle Image Velocity and Infra-Red Thermography.
- Time-averaged temperature distribution for liquid injection in a fluidized bed.
- Effect of droplet size distribution on the bed temperature uniformity.
- Liquid agglomerates observed in the Infra-Red image as cold spots.
- Solids motion affects the liquid distribution in the bed.

ARTICLE INFO

Article history:

Received 29 November 2021

Received in revised form 17 February 2022

Accepted 16 March 2022

Available online 25 April 2022

Keywords:

Infra-Red thermography

Fluidised bed reactors

Heat transport

Non-isothermal

Liquid injection

ABSTRACT

Liquid injection in fluidized beds occurs in well-established industrial processes as fluid coking, spray fluidized bed granulation and condensed mode gas-phase polymerisation. These processes still suffer performance issues due to their complex nature, where liquid injection adds even more complexity.

In this work, the effect of liquid injection on the temperature uniformity in a pseudo-2D fluidized bed was studied using Infra-Red Thermography. The Infra-Red images were also studied to qualify the agglomeration behaviour.

Injecting smaller droplets ($\sim 90 \mu\text{m}$) affects the uniformity of the bed more than injecting larger droplets ($\sim 225 \mu\text{m}$). However, the formation of agglomerates increases with increasing droplet size. The injection velocity influences the average temperature of the bed more for the larger droplets. Additionally, increased solids motion was observed to reduce the agglomeration formation in the bed. Lastly, the particle temperature distribution does not reflect the presence of agglomerates and is thus unsuitable to quantify the agglomeration behaviour.

© 2022 The Authors. Published by Elsevier Ltd. This is an open access article under the CC BY license (<http://creativecommons.org/licenses/by/4.0/>).

1. Introduction

Fluidised bed reactors (FBRs) have been a fundamental building block in process industry for many decades. These units feature good mixing properties, continuous operation, simple design and good heat transfer properties. However, many industrial applications have tailored the original design to better suit the desired process properties. One of these modifications involves injection

of a liquid, which can serve several purposes. In Fluid Coking™ (Oldweiler, 1968), the liquid is a reactant, i.e. a bituminous oil, is injected into the dense solids phase catalyst for cracking. In Spray Fluidised Bed Granulation, the liquid can act as a carrier to deposit solid constituents to achieve particle growth. Liquid injection can also be used for the heat management in the reactor, which is the case for example in Condensed Mode Polymerisation (Duarte Braganca et al., 2000). In these cases, the latent heat of evaporation is used to absorb the heat liberated due to a highly exothermic reaction.

In each of these processes, the injected liquid plays a critical role but it also increases the process complexity. The injected liquid can cause the formation of clusters of particles through the cohesive force of the liquid. The formation of these wet agglomerates can be either detrimental to the process efficiency or be a

* Corresponding author at: Multiphase Reactors Group, Department of Chemical Engineering and Chemistry, Eindhoven University of Technology, P.O. Box 513, 5600 MB Eindhoven, the Netherlands.

E-mail address: m.w.baltussen@tue.nl (M.W. Baltussen).

desired effect. For example, the endothermic reaction in Fluid Coking™ reduces the core temperature of the wet agglomerates, which may induce extensive fouling and consequently cause a premature shutdown of the reactor. Similarly, the agglomeration in Condensed Mode Polymerisation can lead to local cold or hot spots and blockage of the reactor outlet. As opposed to the previous two processes, the particle growth required in spray fluidised bed granulation is achieved through either surface layering or agglomeration.

In both cases, the effect of increased cohesion between the solids has a negative impact on the fluidisation quality, affecting all above stated processes. In most extreme cases, the increased cohesive forces can lead to defluidisation. In addition, Shi et al. found that the wet agglomerates promote the formation of solid bridging, which results in solid agglomerates (Shi et al., 2018). In order to improve the efficiency of processes like the aforementioned, a thorough understanding of the effects of liquid injection is required.

To understand these effects, many studies have focused on the thermal effects and agglomeration behaviour due to liquid injection (Morales et al., 2016; Bruhns and Werther, 2005; Leach et al., 2011; Fries et al., 2011; Book et al., 2011; Shi et al., 2018; Terrazas-Velarde et al., 2011; McDougal et al., 2005; Zhou et al., 2017; Sun et al., 2020). Observing the formed agglomerates without disturbing the process is often complex and costly. For this reason, non-invasive techniques have gained increased interest and are subject to continuous development and improvement. Some of these techniques are Electrical Capacitance Tomography (ECT) (Banaei et al., 2015), X-ray tomography (Kantzas and Kalogerakis, 1996; Yates and Simons, 1994), Magnetic Resonance Particle Tracking (MRPT) or Positron Emission Particle Tracking (PEPT) (Pore et al., 2015) and Particle Image Velocimetry (PIV) (van Buijtenen et al., 2011; De Jong et al., 2012).

The combination of PIV and Infra-Red Thermography (IRT) has been used to study heat transfer (Tsuji et al., 2010; Findlay et al., 2005; Astarita and Carlomagno, 2012; Vollmer and Möllmann, 2017). However, for the use of PIV-IRT visual access into the bed is required, which can be achieved with a pseudo-2D fluidised bed setup. This combination was used by Kolkman et al., who developed a method to study the thermal behaviour in such a fluidised bed (Kolkman et al., 2016; Kolkman et al., 2017). Patil et al. used this technique to study the cooling process of a pseudo-2D fluidised bed (Patil et al., 2015). The technique has also been employed to study reactive systems by Li et al. (Li et al., 2017), who performed adsorption experiments. At low temperatures (30 °C), studies on the effect of the liquid injection on the bed temperature have been reported by Sutkar et al. (Sutkar et al., 2015).

The PIV-IRT method has proven itself to be effective in capturing the whole-field thermal information of the bed. However, the instantaneous character of the measurement combined with the dynamic behaviour of the bed introduces a challenge in capturing the quasi steady state behaviour. In PIV studies of fluidised beds, this behaviour can be captured by time-averaging the measurements. In our previous work (Milacic et al., 2020), the time-averaged results were used to evaluate the particle temperature distribution to qualify/quantify the temperature uniformity of the bed. The distribution and its properties were shown to capture the effects of changing fluidising regimes on the heat transfer properties of the bed. The current experimental work applies the same analysis of the averaged temperature distribution, by means of the standard deviation and the skewness, to study the effect of liquid injection on the temperature uniformity of the bed. Additionally, the agglomeration behaviour is evaluated at varying fluidisation regimes. The same experimental set-up and similar conditions have been used as reported in our previous work (Milacic et al.,

2020). Similarly, this work also uses time-averaged data to ensure accurate representation of the bed.

2. Methods description

2.1. Experimental setup

The fluidisation experiments were performed in a pseudo-2D fluidised bed, of which a schematic representation can be found in Fig. 1. A thorough description of the set-up can be found in our earlier work (Milacic et al., 2020). Therefore only the main characteristics are given here. The bed can be operated in normal fluidisation mode and spouted bed fluidisation mode. The single central spout also acts as a liquid injection nozzle, allowing for liquid injection during spouted bed operation.

The bed is 200 mm in height, 80 mm in width and 15 mm in depth. The bottom consists of a porous metal gas-distributor which includes a single central hole. The liquid injection nozzle is located in the central hole and is on the same level as the surface of the gas-distributor. The spray characteristics can be changed by interchanging the liquid injection needle. More information on the nozzle and spray characteristics can be found in Appendix A. The nozzle that provides a narrow droplet size distribution of very fine droplets will be referred to as the fine spray. The nozzle that provides a wide size distribution of droplet sizes will be referred to as the coarse spray.

The bed is made of PolyMethylMethAcrylate (PMMA) walls, which was chosen for its low thermal conductivity. The front window is made of sapphire glass, because of its transmittance properties in the infra-red spectrum. On the back wall of the bed, a black aluminium plate is placed to increase the contrast between the bubble and emulsion phase.

The gas is humidified nitrogen, its flow rate is controlled with separate mass flow controllers for both the nozzle and gas distributor. The gas streams can be heated separately with gas heaters and the gas-lines after the heaters are traced to reduce heat loss. In this work, the gas velocity from the gas distributor will be

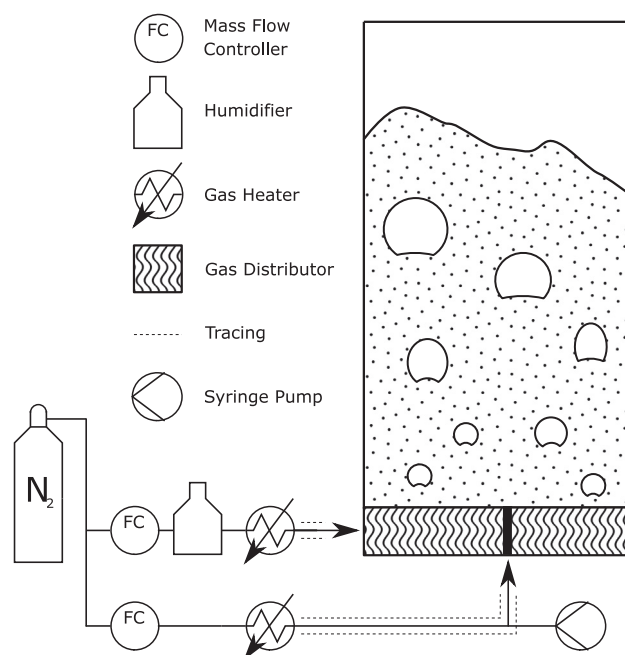


Fig. 1. A schematic representation of the experimental set-up as used in this work.

referred to as background velocity (U_f) and the gas velocity from the nozzle will be referred as the spout velocity (U_{sp}).

Although the gas heaters provide accurate temperature control, the temperature of the bed is still slightly dependent on the gas flow rate. This is due to the gas-distributor housing, which was machined from a solid block of aluminium. Its thermal mass influences the bed temperature, as was discussed in our previous work ((Milacic et al., 2020)). The thermal effect of the aluminium housing on the liquid injection nozzle and its temperature is further discussed in Appendix B. The liquid flow from the nozzle is controlled by a KD Scientific syringe pump (Legato 100 infuse) using a 60 mL Terumo plastic syringe.

2.2. Experimental procedure

The bed in which the experiments take place are composed of either Geldart B or Geldart D particles. These particles are made of glass and have a density of 2526 kg m^{-3} and the sauter mean radii are $591 \pm 138 \mu\text{m}$ and $899 \pm 164 \mu\text{m}$ for Geldart B and Geldart D particles, respectively. The bed loading was 96 mL, which corresponds for both particles to a bed mass of 145 g. The minimum fluidisation (U_{mf}) velocity for both particle types was determined using pressure drop analysis. The U_{mf} for the Geldart B particles is 0.26 m s^{-1} and for the Geldart D particles is 0.53 m s^{-1} . All velocities in this work are normalised by the U_{mf} of the used particles. The fluidisation velocities that were used can be found in Table 1 and have been chosen as in our previous work (Milacic et al., 2020).

At the start of the experiment, the mass flow controllers are set to initiate fluidisation. The gas heaters are used to establish a temperature of approximately 50°C in the reactor under dry fluidisation conditions. Once the bed reached thermal equilibrium, the liquid injection is started, after which the bed is again allowed to reach a steady-state before taking a measurement. After the measurement, the fluidisation parameters are changed and the bed is again allowed to reach a steady-state.

2.3. Data acquisition

In this work, a high speed Infra-Red (IR) camera is used in conjunction with a visual high speed camera, which are synchronised to obtain all whole-field data. The IR-camera is from FLIR (X8400sc) and the visual camera is from PCO (HD DiMAX). To synchronise the cameras to 10 Hz, a digital trigger from Velleman (PCGU 1000) is used.

The visual camera captures the details of the emulsion phase which will be used to determine the solids phase fraction in the bed. This requires good illumination of the bed. The bed temperature distribution is obtained through IR-thermography. This technique converts the detected amount of radiation to a temperature. To achieve this reliably, the measured object, or emitter, should have an emissivity close to 1. The glass particles used have a hemispherical emissivity of $\varepsilon_h = 0.85$ (Rubin, 1985). Using a calibration curve, the amount of radiation can be converted to a temperature.

Table 1

The experimental conditions used in this work: The velocities U_f and U_{sp} are normalised with the minimum fluidisation velocities, which are 0.26 m s^{-1} and 0.53 m s^{-1} for Geldart B and D, respectively. The liquid flow rate Φ_l is in mL min^{-1}

Φ_l	Geldart B		Geldart D	
	U_f	U_{sp}	U_f	U_{sp}
0.00	2.0	28	1.70	15
0.25	3.0	57	1.87	29
0.50		85	2.20	44

Due to the sensitivity of the IR-camera, the camera is placed at an angle to the bed. This angle to bed prevents the IR-camera to capture the temperature difference of the lens in the reflection of the sapphire window of the bed. In addition, this allows the visual camera to be placed in front of the bed.

2.4. Data processing

Although the data acquisition was prepared carefully, some pre-processing is essential. To overlay the images, the viewing angle needs to be corrected. This is done with the method reported by Li et al. (Li et al., 2017). This processing results in an image which angle corrected and cropped to the region of interest.

After correcting the shadows of the visual cropped images, the solids fraction map can be obtained. This is done with the method proposed by de Jong et al. (De Jong et al., 2012). Due to the slight depth of the bed, the images from the IR-camera do not completely overlap the visual images. This is overcome by applying the same subdivision technique as used by de Jong et al. (De Jong et al., 2012).

From the temperature and solids fraction fields, the time-averaged particle temperature distribution can be obtained. This is done using Eq. 1, where T is the local temperature from the temperature field and ε_p is the local solids fraction.

$$\langle T_p \rangle = \frac{\sum_{t=1}^n \varepsilon_p T / \varepsilon_p}{\sum_{t=1}^n \varepsilon_p / \varepsilon_p} \quad (1)$$

This results in a time averaged particle temperature field. The Probability Density Function (PDF) of this field is the particle temperature distribution. Previously, Milacic et al. (Milacic et al., 2020) considered the whole field data when constructing the PDF of the particle temperature. However, a slight error is introduced at higher fluidisation velocities due to disengaged particles in the eruption zone. To correct for this, only the temperature field up to the average bed height is considered. From this new PDF, the standard deviation and skewness have been used to describe the uniformity of the temperature field in the bed, which will also be used to investigate the effects of liquid injection. The standard deviation describes the width of the distribution around the mean value and can be found in Eq. 2.

$$\sigma = \sqrt{\frac{1}{n} \sum_{i=1}^n (T_i - T_{mean})^2} \quad (2)$$

The skewness, Eq. 3 (Joanes and Gill, 1998), describes the asymmetry of the distribution, where a negative value means most samples have a higher value than the mean.

$$\mu_3 = \frac{\frac{1}{n} \sum_{i=1}^n (T_i - T_{mean})^3}{\left[\frac{1}{n-1} \sum_{i=1}^n (T_i - T_{mean})^2 \right]^{3/2}} \quad (3)$$

3. Results

In this work, two different nozzles are used. Allowing for two droplet size distributions and thus varying agglomeration behaviours. These nozzles will be referred to as the fine spray and the coarse spray, resulting in an average droplet size of 90 μm and 220 μm , respectively. Three liquid injection rates are used: $\Phi_l = 0.0 \text{ ml min}^{-1}$, $\Phi_l = 0.25 \text{ ml min}^{-1}$ and $\Phi_l = 0.50 \text{ ml min}^{-1}$.

3.1. Temperature distribution

The results of the fine spray experiments are used to demonstrate the influence of liquid injection rate on the temperature uniformity. To that end, the distribution properties will be compared to the images provided by the IR-camera and the results without injection. A uniform temperature distribution is indicated by a large negative skewness and a low value for the standard deviation (Milacic et al., 2020).

In Fig. 2, three particle temperature distributions are presented, with different liquid injection rates. The temperature profiles are normalised with their respective average bed temperatures, to simplify the visual comparison of the temperature profiles. The matching IR-images are presented in Fig. 3, where the change from black to white indicates an increase in temperature. Due to their relatively low temperature, the presence of agglomerates can be observed in the IR-images as dark regions in the emulsion phase.

With increasing liquid injection rate, the particle temperature distribution changes shape. Increasing the injection rate from $\Phi_l = 0.0$ to $\Phi_l = 0.25$ widens the peak. When increasing the injection rate to $\Phi_l = 0.50 \text{ ml min}^{-1}$, the position of the peak moves below the mean of the distribution. When comparing the IR-images from Fig. 3, a uniform temperature is observed for $\Phi_l = 0.00 \text{ ml min}^{-1}$. When increasing the liquid injection rate to $\Phi_l = 0.25 \text{ ml min}^{-1}$, slight variations can be observed in the emulsion phase as well as a few dark spots. At the highest liquid injection rate of $\Phi_l = 0.50 \text{ ml min}^{-1}$, large agglomerates are visible and the temperature of the emulsion phase is no longer uniform.

Applying the conclusions from the previous work to these observations would imply that, with increasing liquid flow-rate, the standard deviation should increase and the skewness should become less negative. The distribution parameters for these experiments are presented in Fig. 4a and b, where ($U/U_{mf} = 2.13$). Fig. 4a shows that the skewness does behave as predicted in the previous work. However, the standard deviation decreases instead of

increasing, meaning the width of the distribution decreases. This is also observed in Fig. 2.

3.2. Geldart B particles

The experiments discussed above were also performed at higher spout velocities (U_{sp}) and higher background velocities (U_f), as given in Table 1. The results are also presented in Figs. 4a and b. Increasing the spout velocity increases the standard deviation of the temperature distribution, which was also observed in the previous work (Milacic et al., 2020). The skewness generally decreases with increasing spout velocity. This behaviour is more pronounced for experiments with $\Phi_l = 0.50 \text{ ml min}^{-1}$.

For the dry fluidisation, it was found that the standard deviation and skewness are sensible to regime changes (Milacic et al., 2020). These regime changes can cause the non-linear behaviour in the graphs. Additionally, the eruption of particles at higher fluidisation velocities also impact the distribution properties. Although the processing has been adapted for eruption, it only reduces the impact.

To promote the formation of agglomerates, the nozzle was changed for coarser spray, which has a wider droplet size distribution and a larger average droplet size. In practice, this increases the amount of agglomerates in the bed and their size. The results of the experiments with a coarser spray, which sprays the same amount of injected liquid, under the same thermal settings of the reactor are presented in Fig. 5. The standard deviations presented in Fig. 5a span a smaller range compared to the experiments with the fine spray, revealing that larger droplets affect the width of the distribution less than smaller droplets. The skewness values presented in Fig. 5b show a decrease with increasing U_{sp} and an increase with increasing Φ_l . However, the effect of fluidising velocities and liquid injection rate on the skewness seem minor, at higher fluidisation velocities. The temperature uniformity of the bed is not affected. Comparing these results with the results of the fine spray, it seems that a larger average droplet size improves the bed temperature uniformity.

3.3. Geldart D

The experiments performed with the fine spray and the Geldart D particles did not result in liquid agglomeration in the bed. In Table 2 the average temperature, standard deviation and skewness

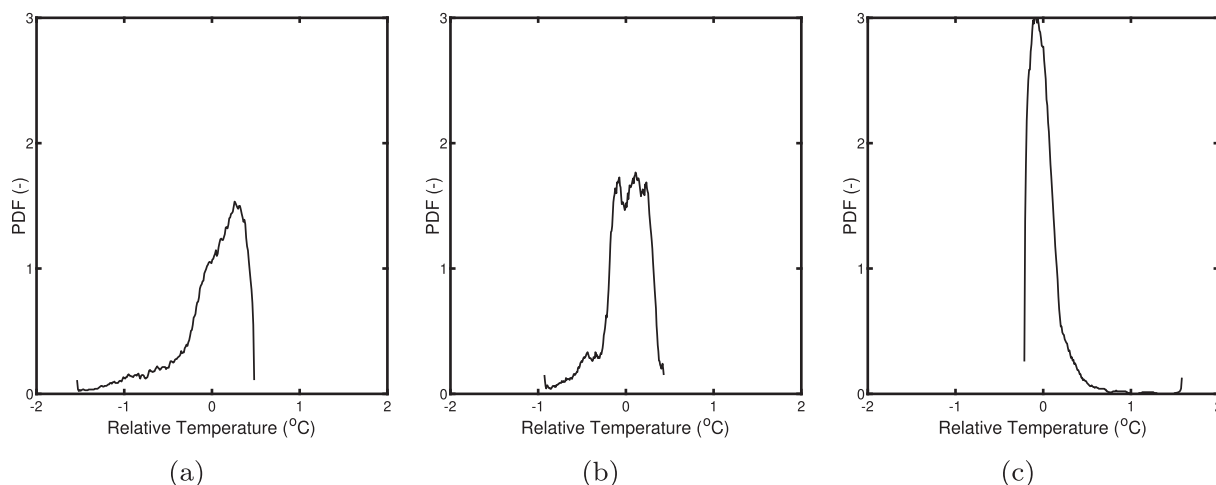


Fig. 2. Particle temperature distributions under influence of varying liquid injection rates, with $U/U_{mf} = 2.13$, Geldart B particles and the fine spray: a. $\Phi_l = 0.00 \text{ ml min}^{-1}$. b. $\Phi_l = 0.25 \text{ ml min}^{-1}$. c. $\Phi_l = 0.50 \text{ ml min}^{-1}$.

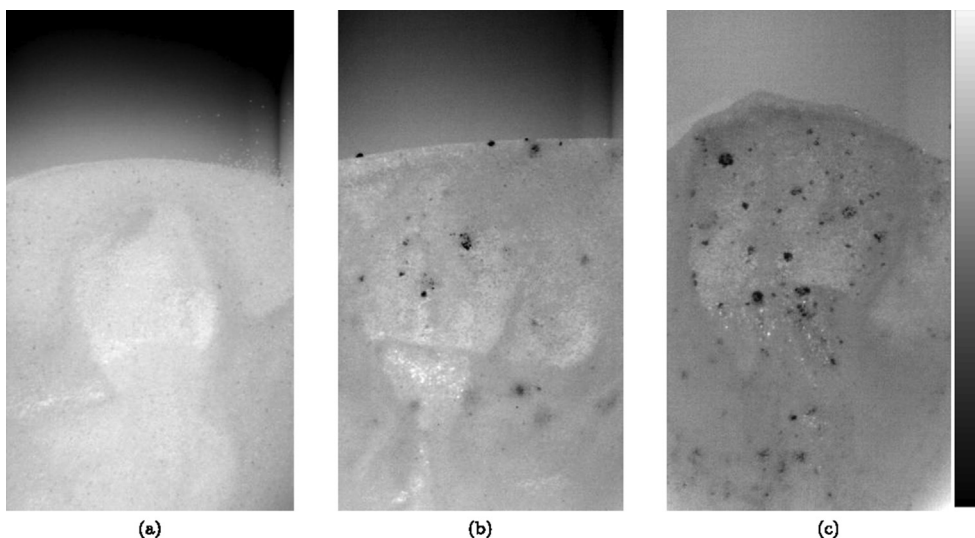


Fig. 3. Cropped IR-images corresponding to the temperature distributions from Fig. 2. Geldart B particles and the fine spray: **a.** $\Phi_I = 0.00 \text{ ml min}^{-1}$. **b.** $\Phi_I = 0.25 \text{ ml min}^{-1}$. **c.** $\Phi_I = 0.50 \text{ ml min}^{-1}$.

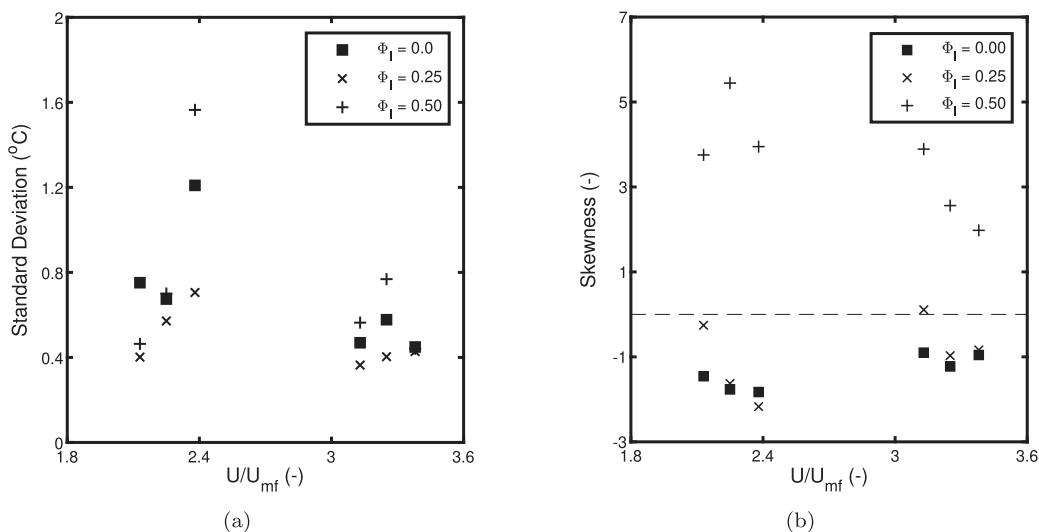


Fig. 4. **a.** Standard Deviation and **b.** Skewness for the experiments with the fine spray and Geldart B particles. For readability, the normalised superficial gas velocity is used to plot the results.

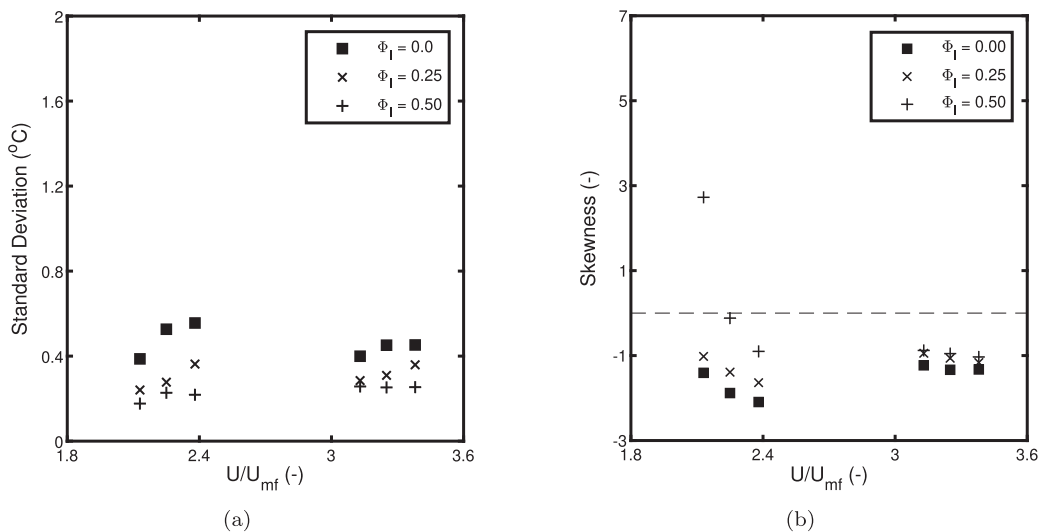
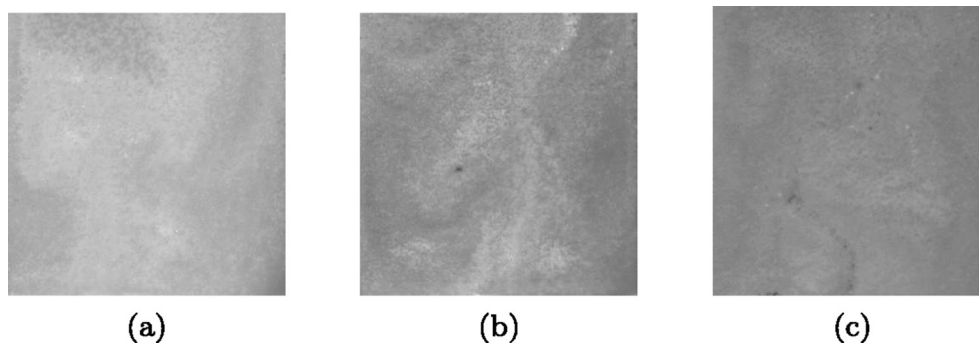
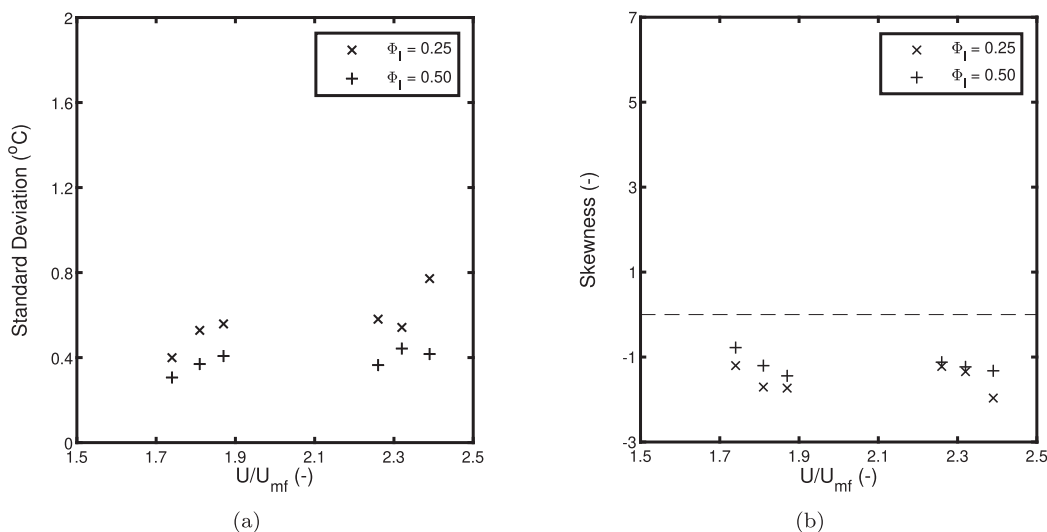


Fig. 5. Standard Deviation and Skewness for the coarser spray with Geldart B particles.

Table 2

Temperature distribution properties for the experiments with the Geldart D particles and the fine spray.

Φ_l	Avg Temp $\langle T \rangle$		STD σ		SKW μ^3	
	U_f 1.87	U_f 2.0	U_f 1.87	U_f 2.0	U_f 1.87	U_f 2.0
0.00	60.5	64.3	1.55	1.74	-2.23	-2.07
0.25	56.2	60.2	0.97	1.26	-1.74	-2.16
0.50	51.2	54.6	1.14	0.90	-2.60	-2.25

**Fig. 6.** Cropped IR-images of the emulsion phase from the experiments with Geldart D particles and the fine spray. $U_f = 1.87$ & $U_{sp} = 15$. **a.** $\Phi_l = 0.00$ ml min^{-1} . **b.** $\Phi_l = 0.25$ ml min^{-1} . **c.** $\Phi_l = 0.50$ ml min^{-1} .**Fig. 7.** Standard Deviation and Skewness for the experiments with the Geldart D particles and the coarse spray.

are presented. Although the average bed temperature decreased by increasing the liquid injection, it did not influence the bed temperature uniformity significantly. The IR-images from Fig. 6 also show that almost no agglomerates were formed.

The experiments with the Geldart D particles and coarser spray resulted in an increased liquid agglomeration rate. However, the effect on the temperature uniformity was minor. Note that for these experiments, different fluidisation velocities were chosen compared to the experiments performed with the fine spray. A larger distance between the two fluidisation velocities was chosen to increase the difference in bubble-induced solids agitation. The standard deviation and skewness are presented in Fig. 7 and show a similar effect as has been observed for the Geldart B particles discussed in the previous section, i.e. a decrease in standard deviation for increasing liquid flow-rate and increase for increasing spout velocity. However for higher velocities, the change in the standard

deviation is not monotonic. The skewness of these experiments are all negative and vary only slightly with the increase of spout velocity or increase in liquid injection rate. The effect of the liquid injection rate and spout velocity only slightly affects the temperature uniformity of the bed.

4. Discussion

4.1. Spout velocity

In the previous section, the particle temperature uniformity of the bed was studied for several process conditions. An increase in U_{sp} generally increases the width of the particle temperature distribution and reduces the value of the skewness. However, the origin of this effect is unclear.

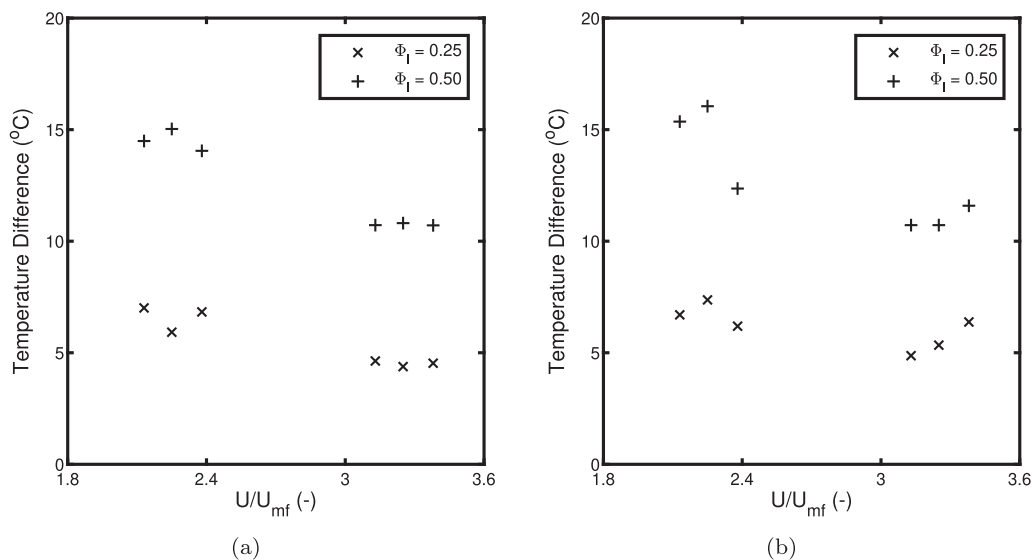


Fig. 8. Temperatures differences for the Geldart B experiments at varying liquid injection rates. **a.** Experiments with the fine spray. **b.** Experiments with the coarse spray.

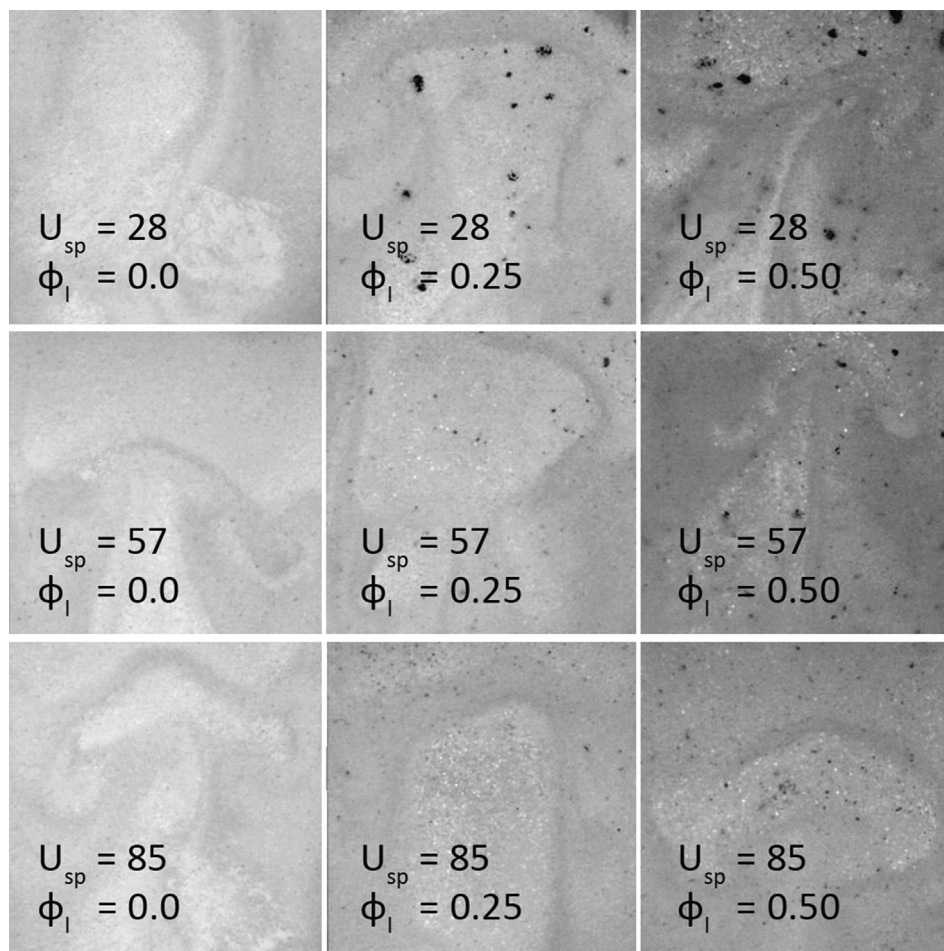


Fig. 9. Cropped IR-images of the emulsion phase from the experiments with the Geldart B particles at $U_f = 3$.

An increased spout gas flow-rate also increases the amount of thermal energy introduced into the system, thus resulting in a higher average bed temperature and improved evaporation.

Besides the thermal effects of the increased U_{sp} , the spouted gas also carries the injected droplets into the bed. At higher flow-rates, the droplets are propelled further into the bed before

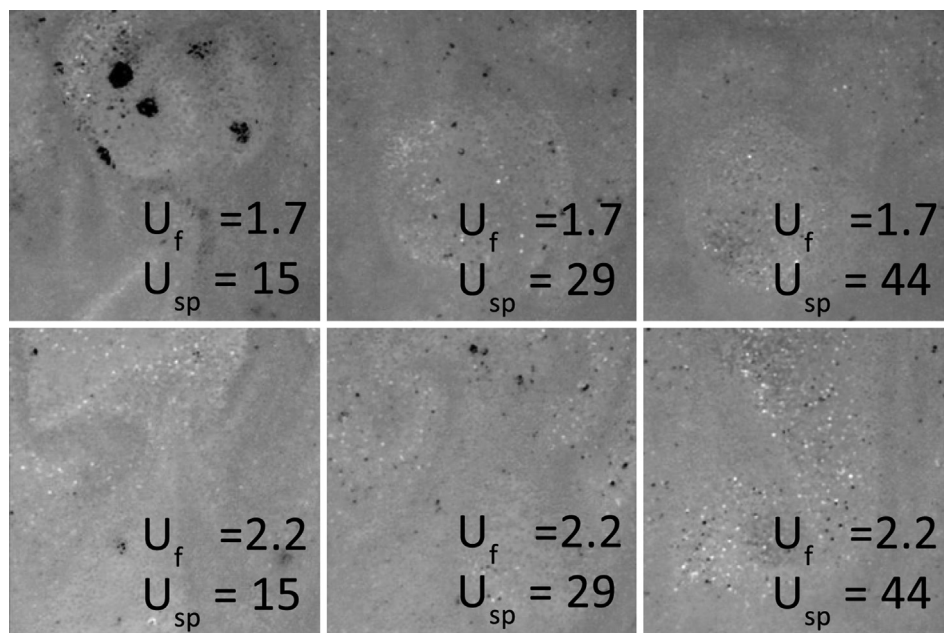


Fig. 10. Cropped IR-images of the emulsion phase from the experiments with the Geldart D particles and $\Phi_l = 0.50 \text{ ml min}^{-1}$.

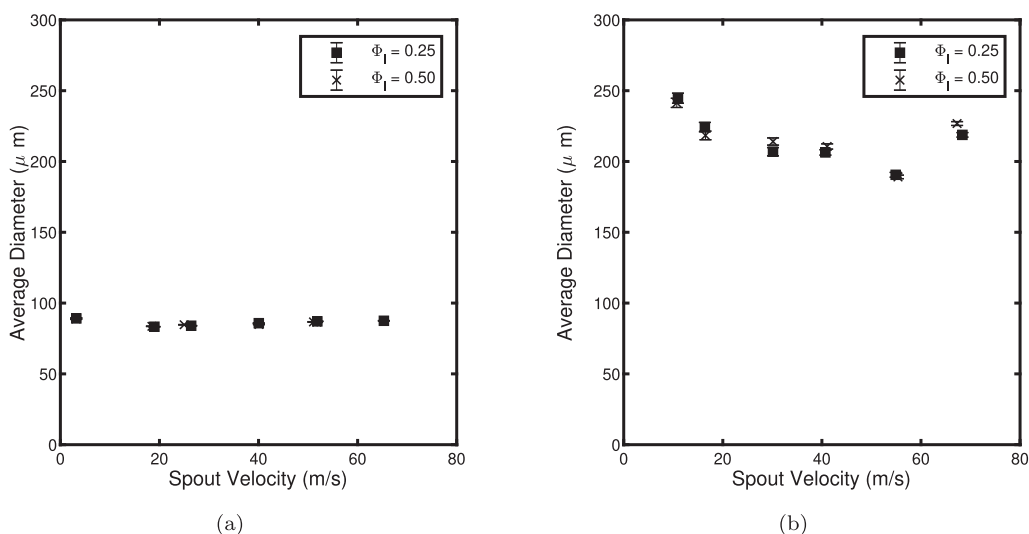


Fig. 11. Droplet size characterisation at varying U_{sp} . **a.** Average droplet size of the fine spray. **b.** Average droplet size of the coarse spray.

colliding with the particles of the emulsion phase. This enlarges the possible collision zone for the droplets, decreasing the local droplet concentration.

It is important to understand the contribution of both the hydrodynamic and thermal effects on the average bed temperature uniformity. To visualise the hydrodynamic effect of the spout on the average bed temperature while excluding the effect of the increased thermal energy, the temperature differences with the $\Phi_l = 0.00 \text{ ml min}^{-1}$ experiments are presented in Fig. 8. The experiments with the fine spray show only slight variations in the temperature difference at lower U/U_{mf} velocities, which are negligible at higher U/U_{mf} velocities. For the experiments with the coarse spray, the hydrodynamic effect has more impact on the average bed temperature, which is increasing with U/U_{mf} . From these results, the increased hydrodynamic effects for the fine spray do not affect the average bed temperature significantly, while for

the coarse spray there is a significant effect. It is also observed that the increased U_f velocity does reduce the temperature difference caused by the injected liquid, this effect is more pronounced for higher liquid injection rates.

4.2. Agglomerate formation

When increasing the average droplet size, the agglomeration rate is increased. For example, no agglomerate formation was observed for experiments with a fine spray and the Geldart D particles while agglomerates are found for the coarse spray. Although the particle temperature distributions with a larger average droplet size are more uniform, agglomerate formation is increased.

Figs. 9 and 10 show IR-images from varying experiments with a large average droplet size and the Geldart B and Geldart D particles. Although the presence of agglomerates can be determined

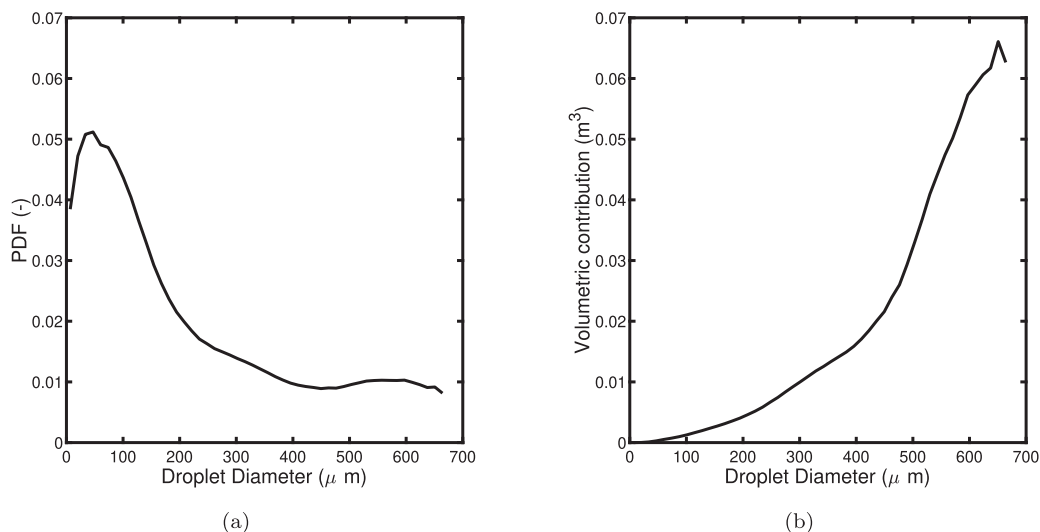


Fig. 12. Spout characterisation of the coarse spray. **a.** Probability Density Function of the droplet size distribution. **b.** Volumetric contribution of the droplet size.

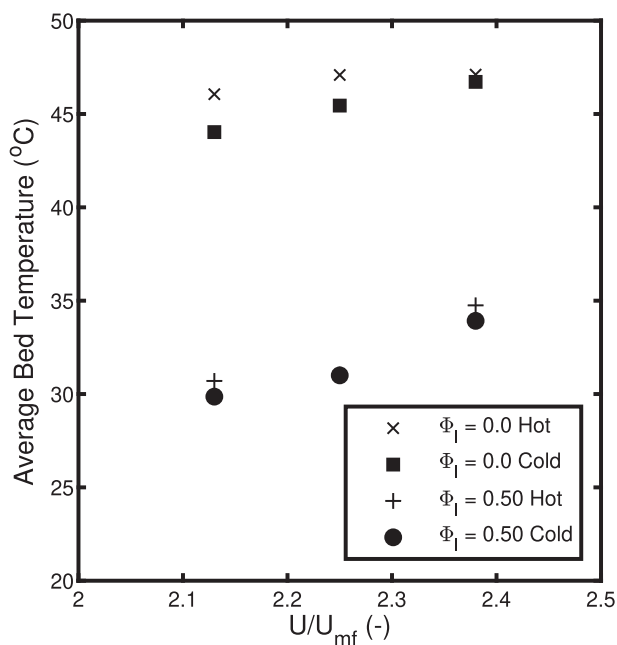


Fig. 13. Effect of nozzle heating on the average bed temperature.

visually, the distribution properties indicate a uniform bed (see values at $U_f = 3$ in Figs. 5a and b). Therefore it can be concluded that the impact of agglomerates on the temperature uniformity is only minor. In addition, the figures show that an increase of liquid injection rate increases agglomerate presence in the bed. This can be counteracted by increasing the superficial gas velocity, because the agglomerates are ruptured by the increased gas velocity.

5. Conclusions

In this work, Infra-Red Thermography was used to study the effect of liquid injection and agglomerate formation in a pseudo-2D fluidised bed. The particle temperature distribution and its properties were used to evaluate the bed temperature uniformity.

The liquid was injected with two different nozzles. One nozzle with a small average droplet size and narrow droplet size distribution and a nozzle with a larger average droplet size and a wide dro-

plet size distribution. The smaller droplet size has a large negative impact on the bed temperature uniformity. The hydrodynamic effect of the spout does affect the relative temperature drop due to the liquid injection, however, only for the averagely larger droplets. Additionally, there is almost no effect of the fine spray in the experiments with Geldart D particles.

A side effect of liquid injection into a fluidised bed is the formation of liquid agglomerates. These liquid agglomerates are observed in the Infra-Red images as dark spots. The Geldart D experiments with the fine spray showed little to no agglomerate formation due to its small average droplet size. The same experiments with a larger average droplet size from the coarse spray, do show agglomeration. Similar results are observed for the experiments with the Geldart B.

Besides, the experiments show that an increase in solids motion decreases the agglomerate size. In addition, the presence and concentration of agglomerates is not reflected by the particle temperature distribution. Thus the particle temperature distribution does not provide a suitable indicator to detect agglomerates in a pseudo-2D fluidised bed, only their thermal influence on the emulsion phase.

CRedit authorship contribution statement

E. Milacic: Software, Validation, Formal analysis, Investigation, Writing – original draft. **M. Nunez Manzano:** Software, Validation, Formal analysis, Investigation, Writing – review & editing. **S. Madanikashani:** Software, Validation, Formal analysis, Investigation, Writing – review & editing. **G.J. Heynderickx:** Writing – review & editing, Supervision, Project administration, Funding acquisition. **K.M. Van Geem:** Writing – review & editing, Supervision, Project administration, Funding acquisition. **M.W. Baltussen:** Conceptualization, Methodology, Software, Validation, Resources, Writing – review & editing, Supervision. **J.A.M. Kuipers:** Conceptualization, Methodology, Software, Validation, Resources, Writing – review & editing, Supervision, Project administration, Funding acquisition.

Declaration of Competing Interest

The authors declare that they have no known competing financial interests or personal relationships that could have appeared to influence the work reported in this paper.

Acknowledgement

This work is part of the Research Programme of the Dutch Polymer Institute (DPI), PO Box 902, 5600 AX, Eindhoven, The Netherlands, project nr. #803.

The research stay of Sepehr Madanikashani at TU/e has received support from the Fund for Scientific Research Flanders (FWO) and the European Regional Development Fund (ERDF) via the PSYCHE project (Interreg France-Wallonie-Vlaanderen) with co-financing from the provinces of East-Flanders and West-Flanders.

The research leading to these results has received funding from the European Research Council under the European Union's Horizon 2020 research and innovation programme/ ERC grant agreement no 818607.

Appendix A. Spout characterisation

In this work, two spray nozzles were used, referred to as the fine spray and the coarse spray. The fine spray has a narrow droplet size distribution with a small droplet size. The coarser spray has a wider droplet size distribution and also a larger average droplet size. The average droplet size was determined using a Phase Doppler Anemometry set-up from Dantec Dynamics. The sprays have been characterised using the same settings as by Finotello et al. (Finotello, 2019). The average size and its dependence on nozzle velocity are presented for both sprays in Fig. 11. It should be noted that the droplet size distribution for the coarse spray is not a normal distribution, its distribution is presented in Fig. 12a. However, the volumetric contribution of the droplet size gives a better understanding of the impact of these few larger droplets. Fig. 12b shows the volumetric contribution in terms of the PDF times the droplet volume. The coarse spray provides a few larger droplets and has been observed to enhance the formation of agglomerates in the bed.

Appendix B. Thermal dependence of the spout

The aluminium housing of the gas distributor, which also houses the nozzle assembly, influences the temperature of the spout. To determine its effect on the bed temperature, six experiments with Geldart B particles were repeated with the gas-heater of the nozzle is turned off. Three of these experiments are performed without liquid injection ($\Phi_l = 0.00 \text{ ml min}^{-1}$) and three are performed with $\Phi_l = 0.50 \text{ ml min}^{-1}$. The recorded average bed temperatures are presented in Fig. 13. The heating of the spout gas seems to have only little effect on the average bed temperature. Therefore it can be concluded that temperature of the injected liquid is mainly dependent on the temperature of the gas-distributor. In addition, the temperature of the gas-distributor is not influenced by the liquid injection, and can thus be considered at constant temperature with changing liquid injection rates and spout velocities. The temperature of the gas-distributor does however increase with increasing background fluidisation velocity.

References

Astarita, T., Carlomagno, G.M., 2012. *Infrared thermography for thermo-fluid-dynamics*. Springer Science & Business Media.
 Banaei, M., van Sint Annaland, M., Kuipers, J.A.M., Deen, N.G., 2015. On the accuracy of landweber and tikhonov reconstruction techniques in gas-solid fluidized bed applications. *AIChE J.* 61 (12), 4102–4113.

Book, G., Albion, K., Briens, L., Briens, C., Berruti, F., 2011. On-line detection of bed fluidity in gas-solid fluidized beds with liquid injection by passive acoustic and vibrometric methods. *Powder Technol.* 205, 126–136.
 Bruhns, S., Werther, J., 2005. An investigation of the mechanism of liquid injection into fluidized beds. *AIChE J.* 51 (3), 766–775.
 De Jong, J.F., Odu, S.O., Van Buijtenen, M.S., Deen, N.G., van Sint Annaland, M., Kuipers, J.A.M., 2012. Development and validation of a novel digital image analysis method for fluidized bed particle image velocimetry. *Powder Technol.* 230, 193–202.
 Duarte Braganca, A.L., Ribeiro de Casto Morschbacker, A.L., Rubbo, E., Neto Miro, C., Barlem, T., Mukherjee, A., 2000. Process for the gas phase polymerization and copolymerization of olefin monomers.
 Findlay, W.P., Peck, G.R., Morris, K.R., 2005. Determination of fluidized bed granulation end point using near-infrared spectroscopy and phenomenological analysis. *J. Pharmaceut. Sci.* 94 (3), 604–612.
 Finotello, G., 2019. Droplet collision dynamics in a spray dryer: experiments and simulations. Ph.D. thesis, Eindhoven University of Technology.
 Fries, L., Dosta, M., Antonyuk, S., Heinrich, S., Palzer, S., 2011. Moisture distribution in fluidized beds with liquid injection. *Chem. Eng. Technol.* 34 (7), 1076–1084.
 Joanes, D.N., Gill, C.A., 1998. Comparing measures of sample skewness and kurtosis. *Royal Stat. Soc.* 47 (1), 183–189.
 Kantzas, A., Kalogerakis, N., 1996. Monitoring the fluidization characteristics of polyolefin resins using x-ray computer assisted tomography scanning. *Chem. Eng. Sci.* 51 (10), 1979–1990.
 Kolkman, T., van Sint Annaland, M., Kuipers, J.A.M., 2016. Development of a non-invasive optical technique to study liquid evaporation in gas-solid fluidized beds. *Chem. Eng. Sci.* 155, 277–293.
 Kolkman, T., van Sint Annaland, M., Kuipers, J.A.M., 2017. Whole-field imaging of temperature and hydrodynamics in a gas fluidized bed with liquid injection. *Chem. Eng. Sci.* 168, 23–40.
 Leach, A., Portoghesi, F., Briens, C., Berruti, F., 2011. A new rapid method for the evaluation of liquid-solid contact resulting from liquid injection into a fluidized bed. *Powder Technol.* 184, 44–51.
 Li, Z., Janssen, T.C.E., Buist, K.A., Deen, N.G., van Sint Annaland, M., Kuipers, J.A.M., 2017. Experimental and simulation study of heat transfer in fluidized beds with heat production. *Chem. Eng. J.* 317, 242–257.
 McDougal, S., Saberian, M., Briens, C., Berruti, F., Chan, E., 2005. Effect of liquid properties on the agglomerating tendency of a wet gas-solid fluidized bed. *Powder Technol.* 149, 61–67.
 Milacic, E., Nunez Manzano, M., Madanikashani, S., Heynderickx, G.J., van Geem, K.M., Baltussen, M.W., Kuipers, J.A.M., 2020. Experimental study on the temperature distribution in fluidized beds. In press at CES.
 Morales, C.B., Jamaledine, T.J., Berruti, F., McMillan, J., Briens, C., 2016. Low-temperature experimental model of liquid injection and reaction in a fluidized bed. *Can. J. Chem. Eng.* 94, 886–895.
 Oldweiler, M.E., 1968. Fluid coking process.
 Patil, A.V., Peters, E.A.J.F., Sutkar, V.S., Deen, N.G., Kuipers, J.A.M., 2015. A study of heat transfer in fluidized beds using an integrated dia/piv/ir technique. *Chem. Eng. J.* 259, 90–106.
 Pore, M., Ong, G.H., Boyce, C.M., Materazzi, M., Gargiuli, J., Leadbeater, T., Sederman, A.J., Dennis, J.S., Holland, D.J., Ingram, A., et al., 2015. A comparison of magnetic resonance, x-ray and positron emission particle tracking measurements of a single jet of gas entering a bed of particles. *Chem. Eng. Sci.* 122, 210–218.
 Rubin, M., 1985. Optical properties of soda lime silica glasses. *Sol. Energy Mater.* 12 (4), 275–288.
 Shi, Q., Li, S., Tian, S., Huang, Z., Yang, Y., Liao, Z., Sun, J., Wang, J., Yang, Y., 2018. Investigating agglomeration behaviours in high temperature gas-solid fluidized beds with liquid injection. *Ind. Eng. Chem. Res.* 57, 5482–5494.
 Sun, J., Tian, S., Li, S., Yang, Y., Huang, Z., Shi, Q., Wang, J., Yang, Y., Wang, F., 2020. Experimental and modeling investigation of liquid-induced agglomeration in a gas-solid fluidized bed with liquid spray. *Ind. Eng. Chem. Res.* 59, 11810–11822.
 Sutkar, V.S., Deen, N.G., Patil, A.V., Peters, E.A.J.F., Kuipers, J., Salikov, V., Antonyuk, S., Heinrich, S., 2015. Experimental study of hydrodynamics and thermal behavior of a pseudo-2d spout-fluidized bed with liquid injection. *AIChE J.* 61 (4), 1146–1159.
 Terrazas-Velarde, K., Peglow, M., Tsotsas, E., 2011. Kinetics of fluidized bed spray agglomeration for compact and porous particles. *Chem. Eng. Sci.* 66, 1866–1878.
 Tsuji, T., Miyauchi, T., Oh, S., Tanaka, T., 2010. Simultaneous measurement of particle motion and temperature in two-dimensional fluidized bed with heat transfer. *KONA Powder Particle J.* 28, 167–179.
 van Buijtenen, M.S., Börner, M., Deen, N.G., Heinrich, S., Antonyuk, S., Kuipers, J.A.M., 2011. An experimental study of the effect of collision properties on spout fluidized bed dynamics. *Powder Technol.* 206 (1–2), 139–148.
 Vollmer, M., Möllmann, K.-P., 2017. *Infrared thermal imaging: fundamentals, research and applications*. John Wiley & Sons.
 Yates, J.G., Simons, S.J.R., 1994. Experimental methods in fluidization research. *Int. J. Multiph. Flow* 20, 297–330.
 Zhou, Y., Shi, Q., Huang, Z., Wang, J., Yang, Y., 2017. Particle agglomeration and control of gas-solid fluidized bed reactor with liquid bridge and solid bridge coupling actions. *Chem. Eng. J.* 330, 840–851.